SUPPLEMENT TO THE *WELDING JOURNAL*, SEPTEMBER 2003
Sponsored by the American Welding Society and the Welding Research Council

Nitrogen Control during the Autogenous Arc Welding of Stainless Steel Part 2: A Kinetic Model for Nitrogen Absorption and Desorption

The influence of three variables on the absorption and desorption of nitrogen during welding is investigated

BY M. du TOIT AND P. C. PISTORIUS

ABSTRACT. This study deals with nitrogen absorption and desorption during the autogenous welding of stainless steel. The influence of the base metal nitrogen and surface-active element concentrations and nitrogen partial pressure in the shielding gas were investigated. The weld nitrogen concentration increased with shielding gas nitrogen content at low-nitrogen partial pressures, but at higher partial pressures, nitrogen absorption was balanced by N_2 evolution. This steady-state nitrogen content was not influenced significantly by the base metal nitrogen content in low-sulfur alloys, but in high-sulphur alloys, an increase in the initial nitrogen concentration caused higher weld nitrogen contents over the entire range of partial pressures evaluated. A kinetic model can be used to describe this behavior. The desorption rate constant decreased with increased sulfur content, but the absorption rate constant was not a strong function of the sulfur concentration. The higher rate of nitrogen removal at the onset of steady-state behavior caused high-nitrogen alloys to require more supersaturation prior to hubble formation.

Introduction

Nitrogen-alloyed austenitic stainless steels offer a unique combination of strength, toughness, and corrosion resistance. This has led to increased interest in these materials in recent years. Although high-nitrogen stainless steels can be welded successfully, nitrogen desorption to the arc atmosphere during autogenous welding has been a cause for concern. This not only creates potential for nitrogen-induced porosity, but a decrease in nitrogen concentration in the region of the weld also has a detrimental effect on the mechanical properties and corrosion resistance of the joint.

Nitrogen absorption and desorption during welding are complex phenomena and, up to this point, no unified theory for the quantitative understanding of the extent of nitrogen dissolution in stainless steels has emerged. This investigation aimed at examining the influence of three variables on the absorption and desorption of nitrogen during the autogenous welding of stainless steel: the shielding gas composition, the base metal nitrogen content prior to welding, and the surface-active element concentration in the weld metal.

During the first phase of this investigation, a number of experimental stainless steels (similar in composition to AISI 310) with varying amounts of nitrogen (approximately 0.005 to 0.27%) and sulphur (about 0.02 and 0.05%) were welded autogenously in pure argon and argon-nitrogen shielding gas atmospheres. The results of this study are considered in a separate publication (Nitrogen Control during the Autogenous Arc Welding of Stainless Steel — Part 1: The Influence of Shielding Gas Nitrogen Content and Base Metal Nitrogen and Sulphur Concentrations on Nitrogen Absorption/Desorption) (Ref. 1) and are summarized below.

KEY WORDS

Absorption
Autogenous
Desorption
Kinetic Model
Nitrogen
Stainless Steel
Sulfur Content

Sievert's law cannot be used to predict the nitrogen content of stainless steel arc welds. At low-nitrogen partial pressures, the weld metal nitrogen content generally exceeds the concentration predicted from equilibrium considerations and increases with an increase in the shielding gas nitrogen content. This enhanced solubility has been reported by several authors and is normally attributed to the presence of monatomic nitrogen in the arc plasma (Refs. 2–5). At higher nitrogen partial pressures in the shielding gas, a dynamic equilibrium is created where the amount of nitrogen absorbed by the weld metal from the arc plasma is balanced by the amount of nitrogen evolved from the weld pool during welding. This steady-state behavior is usually associated with degassing, violent metal expulsion from the weld pool, and excessive spattering.

Nitrogen absorption and desorption reactions during the autogenous welding of nitrogen-alloyed stainless steels were also found to depend on the base metal nitrogen content and the weld surface-active element concentration. In alloys with low surface-active element concentrations, the weld nitrogen content was not

M. du TOIT is Associate Professor, and P. C. PISTORIUS is Professor, Department of Materials Science and Metallurgical Engineering, University of Pretoria, Pretoria, South Africa.

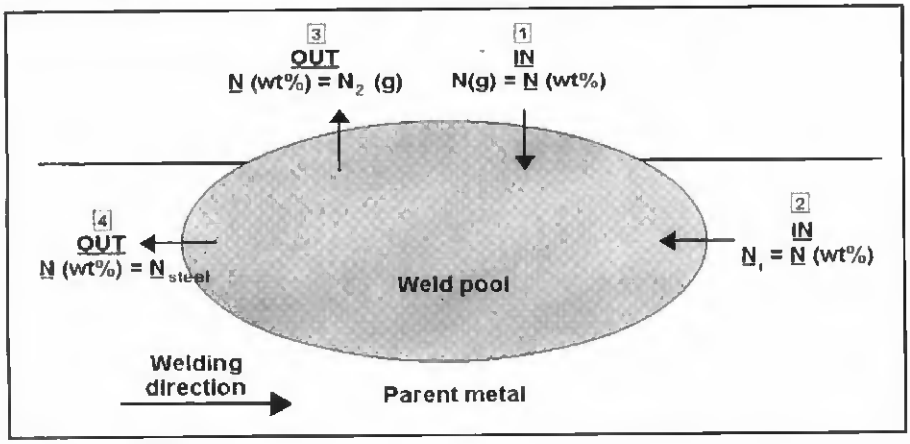

Fig. 1 — Schematic illustration of the proposed kinetic model for the absorption and desorption of nitrogen from autogenous stainless steel weld metal.

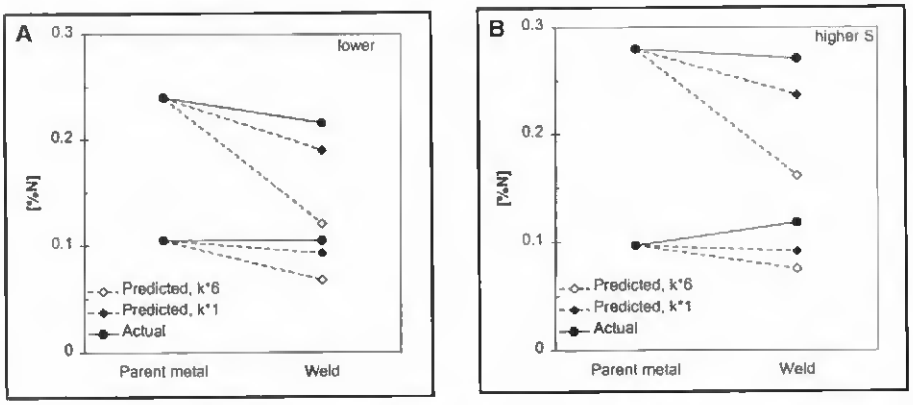

Fig. 2 — Comparison of the actual decrease in nitrogen content from the original base metal composition (filled circles) with the calculated decrease using the rate constant for liquid iron (filled diamonds) and for the case where this rate constant is increased by a factor of 6 (open diamonds). Results shown: A — low-sulfur steel; B — high-sulfur steel. Both welded with pure argon.

influenced to any significant extent by the base metal nitrogen content. In alloys with high surface-active element concentrations, increased base metal nitrogen content resulted in higher weld metal nitrogen contents over the entire range of nitrogen partial pressures evaluated. It is postulated that the weld surface-active element concentration influences the nitrogen absorption and desorption rates by occupying some of the surface sites required for the absorption of monatomic nitrogen from the arc plasma and the recombination of nitrogen atoms to form N_2 (desorption).

The weld metal saturation limit (associated with nitrogen bubble formation) was reached at progressively lower shielding gas nitrogen contents as the base metal nitrogen level increased. This confirms that base metal nitrogen participates in the nitrogen absorption and desorption reactions during welding. Less nitrogen is required in the shielding gas to reach the saturation limit in alloys with high surface-active element concentrations because an appreciable fraction of the nitrogen already present in the base metal is prevented from escaping by the higher level of surface coverage.

In order to justify the conclusions reached in the first phase of this investigation, a suitable theoretical framework is needed. Although a number of thermodynamic models have been developed for nitrogen absorption and desorption during welding, most of these models were derived for pure iron or low-alloy steel welds. Results reported by Kuwana et al. (Ref. 6) suggest that higher chromium contents influence nitrogen absorption/desorption by increasing the equilibrium nitrogen solubility limit in steel. More nitrogen can dissolve in the steel during welding, and reaction rates therefore play an increasingly important role. This suggests that a kinetic approach may be more appropriate than a thermodynamic method for describing the dissolution of nitrogen in high-chromium alloy and stainless steel welds. A kinetic model was therefore developed to quantify the effect of the shielding gas nitrogen content, the base metal nitrogen content prior to welding, and the weld metal surface-active element concentration on nitrogen absorption and desorption during the autogenous arc welding of stainless steel.

Kinetic Model of Nitrogen Absorption and Desorption during Welding

Outline of the Kinetic Model

The proposed kinetic model is illustrated schematically in Fig. 1 and was developed on the basis of the following assumptions:

1) Nitrogen enters the molten weld pool from two sources: the arc atmosphere, i.e., the dissolution of monatomic and diatomic nitrogen from the arc plasma into the liquid metal, and the nitrogen-containing base metal that melts at the leading edge of the weld pool during welding.

2) Dissolved nitrogen is removed from the weld pool by recombining to form nitrogen molecules (N_2), which can escape to the atmosphere, and solidification of nitrogen-containing weld metal at the rear of the weld pool during welding.

3) Under steady-state conditions, the amount of nitrogen entering the weld pool is equal to the amount leaving the weld pool per unit time.

4) The molten weld pool is completely covered by plasma using the welding parameters described in Part 1 (Ref. 1) of this study.

5) The solidification rate at the rear of the pool is proportional to the welding speed.

6) Due to rapid convection in the molten metal, the weld pool is well mixed with a uniform nitrogen concentration. Rapid mass flow also ensures a fairly homogeneous temperature distribution in the molten pool.

7) The model is only valid under conditions where the evolution of nitrogen occurs at the weld pool surface and no bubble formation takes place in the weld metal.

The proposed rate equations for the four nitrogen absorption and desorption processes shown in Fig. 1 are given below.

Nitrogen Entering the Weld Pool from the Arc Atmosphere

The absorption of monatomic nitrogen from the arc plasma, represented by Reaction 1, is best described by a first order rate equation, with the mass transfer rate for this reaction represented by Equation 2.

$$N\,(g) \rightarrow \underline{N}\,(wt\text{-}\%) \qquad (1)$$

$$\frac{dm_N}{dt} = Ak\left[N(g) - \frac{N_{steel}}{K}\right] \quad (2)$$

Where N (wt-%) refers to nitrogen dissolved in the molten weld metal, dm_N/dt is the rate of mass transfer of nitrogen (kg.s^{-1}), A is the weld pool surface area (m^2), k is the reaction rate constant for Reaction 1 (kg.m^{-2}.s^{-1}.atm^{-1}), $N(g)$ is the monatomic nitrogen content of the arc (atm), N_{steel} is the weld nitrogen content (wt-%), and K is the apparent equilibrium constant for Reaction 1.

Nitrogen Entering the Weld Metal through Nitrogen-Containing Base Metal Melting at the Leading Edge of the Pool

If the weld pool has a length L, the time required to melt a volume of metal equal to the volume of the pool is equal to L/v, where v is the torch travel speed. The base metal melting rate (in kg.s^{-1}) is then represented by Equation 3.

$$\text{Melting rate} = \rho V(v/L) \quad (3)$$

Where p is the density of the molten metal (kg.m^{-3}) and V is the weld pool volume (m^3).

The nitrogen mass transfer rate is given by Equation 4.

$$\frac{dm_N}{dt} = \frac{N_i(\text{wt}\%)}{100}\rho V\left(\frac{v}{L}\right) \quad (4)$$

Where N_i is the initial base metal nitrogen content (wt-%).

Nitrogen Leaving the Weld Pool by Recombining to Form N_2

Nitrogen evolution from the weld metal is represented by Equation 5, and the mass transfer rate for this reaction by the second order rate Equation 6.

$$2\underline{N}\ (\text{wt-}\%) \rightarrow N_2\ (g) \quad (5)$$

$$\frac{dm_N}{dt} = -k'A\left(N_{steel}^{\ 2} - K'P_{N_2}\right) \quad (6)$$

Where k' is the reaction rate constant for Reaction 5 (kg.m^{-2}.s^{-1}.[%N]$^{-2}$) and K' is the apparent equilibrium constant for the reaction $N_2\ (g) \rightarrow 2\underline{N}$ (wt-%).

Nitrogen Leaving the Weld Pool through Weld Metal Resolidifying at the Rear of the Pool

Since the solidification rate at the rear of the pool is equal to the melting rate (Equation 3), the rate at which nitrogen leaves the pool by resolidifying is represented by Equation 7.

$$\frac{dm_N}{dt} = -\frac{N_{steel}}{100}\rho V\left(\frac{v}{L}\right) \quad (7)$$

Assumption 3 states that the amount of nitrogen entering the weld pool is equal to the amount leaving the weld pool per unit time under steady-state conditions. From the above, it follows that N_{steel} must be equal to the steady-state nitrogen content, N_{ss}, and the total of Equations 2 and 4 must be equal to the total of Equations 6 and 7 under steady-state conditions.

$$Ak\left[N(g) - \frac{N_{ss}}{K}\right] + \frac{N_i(\text{wt}\%)}{100}\rho V\left(\frac{v}{L}\right) = Ak'\left[N_{ss}^2 - K'P_{N_2}\right] + \frac{N_{ss}}{100}\rho V\left(\frac{v}{L}\right) \quad (8)$$

where N_{ss} is the steady-state nitrogen content (wt-%).

Rearranging Equation 8 to collect all the terms containing N_{ss} on the left yields Equation 9.

$$Ak'N_{ss}^2 + \frac{\rho V}{100}\frac{v}{L}N_{ss} + Ak\frac{N_{ss}}{K} = Ak'K'P_{N_2} + AkN(g) + \frac{v}{L}\frac{\rho V}{100}N_i(\text{wt}\%) \quad (9)$$

For a specific shielding gas composition and set of welding parameters, the weld pool area A, length L, and volume V; the monatomic nitrogen content of the arc $N(g)$; the welding speed v; the density p; the equilibrium constants K and K'; and the nitrogen partial pressure in the shielding gas P_{N_2} should remain constant regardless of the base metal nitrogen content and the surface-active element concentration in the weld metal. The following conclusions can now be drawn:

According to Equation 9, the steady-state nitrogen content, N_{ss}, is a function of the base metal nitrogen content N_i, with an increase in base metal nitrogen concentration leading to an increase in the steady-state nitrogen content. This was observed experimentally, as shown in Figs. 2 and 3 in Part 1 (Ref. 1). The extent of this dependence, however, is determined by the magnitude of the two reaction rate constants, k (for the absorption reaction) and k' (for the desorption reaction). Earlier results suggested that the desorption rate constant varies with the surface-active element concentration in the weld metal. In the low-sulfur steels, desorption of nitrogen from the weld pool is rapid, leading to high values of k', whereas desorption is retarded in the high-sulfur alloys, resulting in low k' values. The absorption rate constant, k, is not expected to be a strong function of the surface-active element concentration.

Given the low desorption rate constant in the high-sulfur alloys, Equation 9 suggests that the steady-state nitrogen content is a strong function of the base metal nitrogen content, with N_{ss} increasing as N_i increases. This is consistent with the results shown in Fig. 3 of Part 1. In the low sulfur alloys, k' is expected to be higher and gas-metal (or plasma-metal) reactions should, therefore, play a more significant role in determining the steady-state nitrogen content. According to Equation 9, the influence of the base metal nitrogen content on the steady-state weld metal nitrogen level is less pronounced at high k' values. This is consistent with the results shown in Fig. 2 of Part 1.

Values of the Constants

In order to use Equation 9 to predict the nitrogen content of the experimental alloys after welding, a number of constants, including the partial pressure of monatomic nitrogen in the arc $N(g)$, the weld pool surface area A, volume V, and length L; the density of the molten metal p; the two apparent equilibrium constants for the absorption and desorption reactions K and K'; and the two reaction rate constants k and k'; have to be determined. The values of these constants were measured experimentally or calculated using relationships obtained from published literature.

Partial Pressure of Monatomic Nitrogen in the Arc

The partial pressure of monatomic nitrogen in the arc was estimated using the method developed by Mundra and DebRoy (Ref. 7) and Palmer and DebRoy (Ref. 8). These authors derived Equation 11 for calculating the partial pressure of monatomic nitrogen formed as a result of the dissociation of molecular nitrogen, Reaction 10, at a hypothetical temperature T_d in the arc plasma. T_d is defined as the dissociation temperature at which the equilibrium thermal dissociation of diatomic nitrogen in the arc would produce the actual partial pressure of monatomic nitrogen present in the plasma. The authors concluded that T_d is approximately 100 K higher than the weld pool surface temperature.

$$\tfrac{1}{2}N_2\ (g) \rightarrow N\ (g) \quad (10)$$

Table 1 — Estimated Monatomic Nitrogen Partial Pressure in the Arc Atmosphere

Shielding Gas Nitrogen Content	Nitrogen Partial Pressure, P_{N_2}	Monatomic Nitrogen Partial Pressure, P_N	Equilibrium Nitrogen Content, N_{eq}
1.09%	0.0094 atm	8.43×10^{-8} atm	0.0200 wt-%
5.3%	0.0456 atm	1.86×10^{-7} atm	0.0442 wt-%
9.8%	0.0843 atm	2.53×10^{-7} atm	0.0601 wt-%
24.5%	0.2107 atm	4.00×10^{-7} atm	0.0950 wt-%

Note: Monatomic partial pressure estimated for an effective plasma temperature of 2628 K and the equilibrium nitrogen content of the weld metal at a weld pool temperature of 1722°C.

Table 2 — Weld Pool Dimensions

Weld pool surface area	34.1 ± 4.8 mm²
Weld pool length	7.4 ± 0.5 mm
Weld pool volume	63.9 ± 6.3 mm³

Note: 95% confidence interval.

$$P_N = \sqrt{P_{N_2}}\, exp\left(-\frac{\Delta G^{\circ}_{10,T_d}}{RT_d}\right) \quad (11)$$

Where P_N is the partial pressure of monatomic nitrogen in the arc (atm), $\Delta G^{\circ}_{10,Td}$ is the standard free energy for Reaction 10 at T_d, and R is the universal gas constant (8.314 J.K^{-1}.mol^{-1}).

Since the extent of dissociation of diatomic nitrogen is low under typical welding conditions, P_{N_2} can be assumed to be equal to the partial pressure of N_2 in the inlet gas. The free energy of formation of monatomic nitrogen from N_2, $\Delta G^{\circ}_{10,Td}$, used by Mundra and DebRoy (Ref. 7) and Palmer and DebRoy (Ref. 8), was obtained from the compilation by Elliott and Gleiser (Ref. 9). However, the data in this reference appears to be in error, specifically with regards to the heat of formation of N from N_2. Elliott and Gleiser quote a value of 358.0 kJ/mol (of N), whereas Kubaschewski et al. (Ref. 10) report 472.7 kJ/mol. The latter value agrees exactly with the bond strength of the diatomic molecule of 945.44 kJ/mol (of N_2) (Ref. 11).

One implication of this is that the conclusion of Palmer and DebRoy that the effective plasma temperature (as regards the dissociation of N_2) is 100°C higher than the metal surface temperature, is in error, because this conclusion was based on the data of Elliott and Gleiser. In the current investigation, this inaccuracy was corrected by recalculating the "effective dissociation temperature" as that temperature that yields — for the conditions of the Palmer and DebRoy experiments — the same partial pressure of monatomic nitrogen when the Kubaschewski et al. data are used, as does the Elliott and Gleiser data at a temperature of 1400°C, which is 100°C higher than the surface temperature in the Palmer and DebRoy investigation. This yields a reassessed effective plasma temperature that is 633°C higher than the surface temperature — much higher than the value reported by Palmer and DebRoy.

If the surface temperature of the weld pool is assumed to be approximately equal to the measured weld pool temperature of 1722°C (refer to Part 1), the values of P_{N2}, $\Delta G^{\circ}_{10,Td}$, T_d, and R can be substituted into Equation 11, and the partial pressure of monatomic nitrogen in the arc plasma can be estimated for all the shielding gas atmospheres used in this investigation. The estimated monatomic nitrogen partial pressures are shown in Table 1, taking into consideration that total atmospheric pressure in Pretoria, where the experiments were performed, is 0.86 atm.

Data in Table 1

The Weld Pool Surface Area *A*, Length *L*, and Volume *V*

The area and length of the weld pool were estimated by assuming that the crater at the end of each weld bead, where insufficient liquid metal was present to fill the depression created by the arc jet, has the same dimensions as the weld pool during welding. In order to determine these dimensions, the end craters of seven weld beads were photographed, and the area and maximum length of each crater were measured. The average values of the weld pool length and area determined using this method are shown in Table 2.

Data in Table 2

The volume of the weld pool was estimated by sectioning a number of weld beads and photographing polished and etched cross sections. If it is assumed that the weld pool has the shape of a section of a sphere, Equation 12 can be used to calculate the weld pool volume (Ref. 12). The average weld pool volume determined using this method is shown in Table 2.

$$V = \frac{1}{3}\pi r^3\left(2 - 3\cos\theta + \cos^3\theta\right) \quad (12)$$

Where r is the radius of the sphere, and θ is the angle between the fusion line and the plate at the surface of the sample.

The Apparent Equilibrium Constants *K* and *K'*

The Apparent Equilibrium Constant for the Desorption Reaction *K'*

If nitrogen desorption from the weld pool during welding is represented by Equation 5, the apparent equilibrium constant K' for this reaction is given by Equation 13.

$$K' = \frac{\left[N_{eq}(\text{wt\%})\right]^2}{P_{N_2}} \quad (13)$$

Where N_{eq} is the equilibrium N content of the molten metal at the weld pool temperature (wt-%).

The equilibrium nitrogen content as a function of temperature can be calculated using Wada and Pehlke's results and Equation 14 (Ref. 13).

$$\log\left(N_{eq}\right) = -\frac{247}{T} - 1.22 - \left(\frac{4780}{T} - 1.51\right)\log f_{N,1873} - \left(\frac{1760}{T} - 0.91\right)\left(\log f_{N,1873}\right)^2 \quad (14)$$

Where T is the temperature (K) and $f_{N,1873}$ is the nitrogen activity coefficient at 1873 K.

The activity coefficient, f_N, is calculated from the composition of the steel using Equation 15 (Ref. 13).

$$\begin{aligned}\log f_N = {} & \{-164[\%Cr] + 8.33[\%Ni] - 33.2[\%Mo] \\ & - 134[\%Mn] + 1.68[\%Cr]^2 - 1.83[\%Ni]^2 \\ & - 2.78[\%Mo]^2 + 8.82[\%Mn]^2 + (1.6[\%Ni] \\ & + 1.2[\%Mo] + 2.16[\%Mn])\{\%Cr\} \\ & + (-0.26[\%Mo] + 0.09[\%Mn])\{\%Ni\}\}/T \\ & + \{0.0415[\%Cr] + 0.0019[\%Ni] \\ & + 0.0064[\%Mo] + 0.035[\%Mn] \\ & - 0.0006[\%Cr]^2 + 0.001[\%Ni]^2 \\ & + 0.0013[\%Mo]^2 - 0.0056[\%Mn]^2 \\ & + (-0.0009[\%Ni] - 0.0005[\%Mo] \\ & - 0.0005[\%Mn])\{\%Cr\} + (0.0003[\%Mo] \\ & + 0.0007[\%Mn])\{\%Ni\}\} + 0.13[\%C] \\ & + 0.06[\%Si] + 0.046[\%P] + 0.007[\%S] \\ & + 0.01[\%Al] - 0.9[\%Ti] - 0.1[\%V] \\ & - 0.003[\%W] - 0.12[\%O]\end{aligned} \quad (15)$$

Where [%M] is the alloying element content in wt-%.

For the experimental alloys, calculation yields the equilibrium nitrogen contents shown in Table 1 at a weld pool temperature of 1722°C, taking into consideration

total atmospheric pressure in Pretoria is 0.86 atm. These values were substituted into Equation 13 to yield an average apparent equilibrium constant of 4.28×10^{-2} for the nitrogen desorption reaction.

The Apparent Equilibrium Constant for the Absorption Reaction K

The apparent equilibrium constant, K, for the nitrogen dissolution reaction (Equation 1) is represented by Equation 16. The relationship between K, K', and K_1 (the equilibrium constant for the dissociation of diatomic nitrogen) is shown in Equation 17 with the equilibrium constant, K_1, for nitrogen dissociation (Reaction 10) given by Equation 18.

$$K = \frac{N_{eq}}{P_N} \tag{16}$$

Where N_{eq} is the nitrogen concentration in equilibrium with the monatomic nitrogen in the arc.

$$K = \frac{\sqrt{K'}}{K_1} \tag{17}$$

$$\text{where} \qquad K_1 = \frac{P_N}{\sqrt{P_{N_2}}} \tag{18}$$

Since P_{N_2} and K' are known, and the partial pressure of monatomic nitrogen in the arc plasma at the weld pool temperature can be determined, K can be calculated. Calculation yields an average K value of 2.55×10^8 at the weld pool temperature of 1722°C. K_1, the equilibrium constant of Reaction 10, was calculated from the data of Kubaschewski et al. (Ref. 10).

The Nitrogen Desorption and Absorption Rate Constants, k' and k

The Nitrogen Desorption Rate Constant, k'

Correlations based on the reaction rate of diatomic nitrogen with pure iron from the summaries of Belton (Ref. 14) and Turkdogan (Ref. 15) were used to estimate the rate constant for nitrogen desorption from the weld pool as N_2 (Reaction 5). For the reaction $N_2(g) \rightarrow 2\underline{N}$ (wt-%), the rate constant (for temperatures ranging from 1550 to 1700°C) is given by Equation 19.

$$k_1 = \frac{10^{\left(-6340/T + 1.85\right)}}{1 + 260 f_o [\%O] + 130 f_s [\%S]} \quad \text{g.cm}^{-2}.\text{min}^{-1}.\text{atm}^{-1} \tag{19}$$

Table 3 — Calculated Values of the Rate Constant k for the Absorption of Dissociated Nitrogen by the Weld Pool

Alloy	Comments	Base Metal Nitrogen Content	Sulphur Content	$10^{-3}k$ (kg . m^{-2} . s^{-1} . atm^{-1})
a) Rate constant k' for liquid iron				
VFA 657	Low N, low S	0.005	0.023	38
VFA 658	Medium N, low S	0.105	0.023	43
VFA 659	High N, low S	0.240	0.022	35
VFA 752	Low N, high S	0.006	0.052	36
VFA 753	Medium N, high S	0.097	0.061	30
VFA 755	High N, high S	0.280	0.049	27
b) Rate constant k' taken to be 6 times that for liquid iron				
VFA 657	Low N, low S	0.005	0.023	57
VFA 658	Medium N, low S	0.105	0.023	124
VFA 659	High N, low S	0.240	0.022	210
VFA 752	Low N, high S	0.006	0.052	46
VFA 753	Medium N, high S	0.097	0.061	61
VFA 755	High N, high S	0.280	0.049	159

Where f_o and f_s are the activity coefficients of dissolved oxygen and sulfur, respectively, and [%O] and [%S] are the mass percentages of dissolved oxygen and sulfur, respectively.

The rate expression used with this rate constant is as follows:

$$\frac{dm_N}{dt} = k_1 A \left[P_{N_2} - \frac{N_{steel}^2}{K'} \right] \tag{20}$$

Comparison with Equation 6 shows that $k' = k_1/K'$.

For stainless steels, the activity coefficient of sulfur, f_s, can be estimated as follows (Ref. 16):

$$\log f_s = [\%Cr]\left(-\frac{94.2}{T} + 0.040 \right) \tag{21}$$

where [%Cr] is the mass percentage of chromium in the steel. For a weld pool temperature of 1722°C and an average chromium content of 24.4%, this yields a value of $f_s = 0.67$ for the experimental alloys.

In these calculations, the effect of dissolved oxygen on the rate constant was neglected since no data were available on oxygen levels. However, the activity of oxygen is expected to be low in chromium-rich steels, and since the sulfur levels are comparatively high, neglecting the effect of dissolved oxygen is not expected to affect the calculations significantly.

Substitution of the constants and unit conversion yield the following expression for the rate constant, for a temperature of 1722°C:

$$k' = \frac{0.183}{1 + 87[\%S]} \ \text{kg} \cdot \text{m}^{-2} \cdot \text{s}^{-1} \cdot (\%)^{-2} \tag{22}$$

This expression for the desorption rate constant is valid for liquid iron. For stainless steels, the rate constant for this reaction is generally larger than that for liquid iron by a factor of about 6 (Refs. 14, 17). However, this conclusion is based on experiments conducted at 1600°C and leads to an overestimate in this investigation. Part of the reason for choosing not to increase the rate constant over that for pure iron is illustrated in Fig. 2, which compares the measured and predicted reduction in the weld nitrogen content for welding under pure argon. When welding in pure argon, no monatomic nitrogen is assumed to form in the plasma, and hence, the (unknown) absorption rate constant k has no effect on the weld nitrogen content that is calculated using Equation 9. As the figure shows, both values of the rate constant k' overpredict the decrease in the weld nitrogen content, but the correspondence is much better for the smaller rate constant.

Explaining Figure 2

Based on these conclusions, Equation 22 yields values for the desorption rate constant, k', of 6.28×10^{-2} and 3.21×10^{-2} kg·m^{-2}s^{-1}·(%)$^{-2}$ for the low- and high-sulfur alloys, respectively. The reduction in the desorption rate constant at higher surface-active element concentrations is consistent with a site blockage model, where sulfur atoms are assumed to occupy a fraction of the surface sites required for the adsorption of nitrogen.

The Nitrogen Absorption Rate Constant k

No literature data on the value of the rate constant k for the reaction of monatomic nitrogen with stainless steel were found. This constant was, therefore,

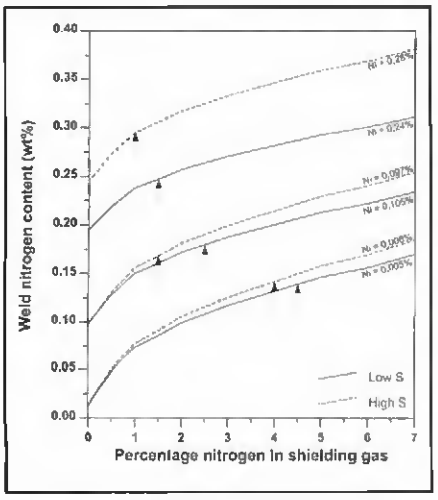

Fig. 3 — Predicted change in weld nitrogen content for shielding gases that are increasingly rich in nitrogen. Calculated for the base metal compositions of the experimental alloys. The arrows indicate the minimum shielding gas compositions where bubbling was observed experimentally.

Table 4 — Summary of the Constants Required in Equation 9

Constant	Values
P_N	8.43×10^{-8} atm if $P_{N_2} = 0.0094$ atm
	1.86×10^{-7} atm if $P_{N_2} = 0.0456$ atm
	2.53×10^{-7} atm if $P_{N_2} = 0.0843$ atm
	4.00×10^{-7} atm if $P_{N_2} = 0.2107$ atm
A	34.1 mm^2
L	7.4 mm
V	63.9 mm^3
K	2.55×10^8
K'	4.28×10^{-2}
ρ	6755 kg . m^{-3}
v	2.7 mm . s^{-1}
k	3.5×10^4 kg . m^{-2} . s^{-1} . atm^{-1}
k'	6.28×10^{-2} kg . m^{-2} . s^{-1} . (%)$^{-2}$ for the low sulphur alloys
	3.21×10^{-2} kg . m^{-2} . s^{-1} . (%)$^{-2}$ for the high sulphur alloys

estimated from the experimental data, using Equation 9 for the case where the shielding gas contained 1.09% nitrogen (nitrogen bubbles formed at higher nitrogen contents, rendering one of the assumptions on which the model is based invalid). Calculated values of the absorption rate constant are summarized in Table 3.

Data of Table 3

As shown in Table 3, use of the larger rate constant k' yields values for the constant k, which seem to depend on the initial nitrogen content of the steel. There appears to be no fundamental reason why this should be the case. When the rate constant k' for liquid iron is used in its original form, the rate constant k is approximately the same for all the steels. Interestingly, no strong effect of the sulfur content on the rate constant for dissociated nitrogen was found. This is in contrast with the case for the reaction that involves molecular nitrogen, where an increase in sulfur from 0.022 to 0.054% causes a decrease in the rate constant k' by a factor of approximately 2. Given the weak dependence of k on steel composition, an average value of 3.5×10^4 kg.m^{-2}.s^{-1}.atm^{-1} was used in the subsequent calculations (together with the value of k' as for liquid iron).

A summary of all the constants required for substitution into Equation 9 is given in Table 4.

Explaining Figure 3

Predicted Weld Nitrogen Concentration

Figure 3 shows the predicted weld nitrogen concentration as a function of the shielding gas nitrogen content for the experimental alloys. The predicted behavior is close to that found experimentally (shown in Figs. 2 and 3 in Part 1), with marked increases in weld nitrogen content at low-nitrogen partial pressures. The influence of the base metal nitrogen content and the surface-active element concentration is also consistent with that observed experimentally.

The results shown in Fig. 3 are only valid until the onset of bubble formation. Beyond this point, nitrogen is removed from the weld pool not only by the gas-metal reaction at the weld pool surface but also by bubble formation within the pool. This condition is not covered by the simple kinetic model presented here. For shielding gas compositions at the onset of bubbling, the predicted rates at which nitrogen enters and leaves the pool by means of the four mechanisms considered in the model are summarized in Table 5. This shows that the main mechanism by which nitrogen enters the pool is a function of the initial base metal nitrogen content, with nitrogen absorption from the arc playing a dominant role at low base metal nitrogen contents, and melting of nitrogen-containing base metal at high initial nitrogen levels. The main exit mechanism appears to be nitrogen leaving the weld metal through solidification, rather than nitrogen desorption to the atmosphere. It is evident from Fig. 3 that higher sulfur concentrations slightly retard the desorption of N_2 to the atmosphere (giving higher nitrogen contents in the weld pool for a similar base metal nitrogen content). This is consistent with the site blockage model described earlier.

Data in Table 5

Two factors are of interest in the practical welding situation: the change in nitrogen content upon welding, and the formation of nitrogen bubbles. The former situation appears to be fairly well described by the kinetic model. However, the latter is more difficult to predict. As Figs. 2 and 3 in Part 1 show, bubble formation was observed for weld nitrogen contents ranging from 0.16 to 0.29%. In comparison, the equilibrium nitrogen content for a nitrogen partial pressure of 0.86 atm (atmospheric pressure in Pretoria) is 0.19% at 1722°C. (The saturation concentration depends somewhat on temperature).

For the formation of a nitrogen bubble in the weld pool, the nitrogen partial pressure within the bubble must at least equal atmospheric pressure (in fact, it must be slightly higher to compensate for the surface tension of the bubble). Considering that the nitrogen saturation content is 0.19%, the high-nitrogen alloys display a significant degree of supersaturation prior to the onset of bubble formation. This is consistent with the results of Blake and Jordan (Ref. 18), who reported that the steady-state nitrogen content of molten iron is in excess of that required to provide an internal pressure of one atmosphere at the assumed temperature of the liquid metal. The increased levels of supersaturation for the higher-nitrogen alloys are presumably related to the higher rate of nitrogen removal as N_2 at the onset of bubble formation (as is evident from Table 5). Given that nitrogen bubble formation and detachment require bubble nucleation and growth, it appears reasonable to assume that a higher nitrogen removal rate (as bubbles) would require a higher degree of supersaturation (a larger "driving force"). Such a link between supersaturation and the nitrogen removal rate is also evident in the experimental results shown in Figs. 2 and 3 (Part 1), where the weld nitrogen concentration increases if the shielding gas nitrogen content is increased beyond the onset of bubble formation.

On the other hand, it does not appear possible to form bubbles at weld nitrogen contents below 0.19%, as was found experimentally for most of the lower-nitrogen alloys. Possible reasons for this discrepancy include deviation of the weld pool temperature from that measured, deviation of the actual saturation concentration of nitrogen from that predicted by the correlation for f_N, and errors in chemical analysis.

Conclusions

A kinetic model can be used to describe nitrogen absorption and desorption during the welding of the experimental stainless

Table 5 — Relative Contributions of the Four Reactions that Add or Remove Nitrogen to or from the Weld Pool

Alloy	Comments	$\frac{dN(wt\text{-}\%)}{dt}$, mg · s^{-1} (1) Absorption of Monatomic N from Plasma	(2) Melting of Base Metal at Leading Edge of Weld Pool	(3) Desorption of N_2 from the Weld Pool	(4) Solidification at the Rear of the Weld Pool
VFA 657	Low N, low S	0.203	0.008	–0.025	–0.185
VFA 658	Medium N, low S	0.151	0.165	–0.055	–0.261
VFA 659	High N, low S	0.116	0.378	–0.120	–0.374
VFA 752	Low N, high S	0.191	0.009	–0.014	–0.187
VFA 753	Medium N, high S	0.117	0.153	–0.024	–0.246
VFA 755	High N, high S	0.095	0.441	–0.093	–0.442

Note: The reactions are at the respective shielding gas compositions where bubble formation was observed experimentally.

steels. The proposed model considers the absorption of monatomic nitrogen from the arc plasma, the evolution of N_2 from the weld pool, nitrogen entering the weld metal through the melting of nitrogen-containing base metal, and nitrogen leaving the weld pool through the solidification of weld metal at the rear of the pool. The predictions of the model show good agreement with the experimental results discussed in Part 1 of this investigation.

The calculated nitrogen desorption rate constant is a function of the surface-active element concentration in the alloy, with the rate constant decreasing at higher concentrations of sulfur in the steel. This is consistent with a site blockage model, where surface-active elements occupy a fraction of the surface sites required for nitrogen adsorption. The rate constant for the absorption of dissociated nitrogen is, however, not a strong function of the surface-active element concentration.

The main mechanism by which nitrogen enters the weld pool is dependent on the initial nitrogen content of the alloy, with nitrogen absorption from the arc plasma playing a dominant role at low base metal nitrogen contents, and the melting of nitrogen-containing base metal at high initial nitrogen levels. The main exit mechanism appears to be nitrogen leaving the pool due to the solidification of nitrogen-containing weld metal at the rear of the weld pool rather than nitrogen desorption to the atmosphere as N_2.

Although the minimum shielding gas nitrogen content that leads to bubbling cannot be determined from the model, it is evident that some supersaturation above that required to nucleate nitrogen bubbles in the melt occurs in the high-nitrogen alloys. This can probably be attributed to the higher rate of nitrogen removal as N_2 at the onset of bubble formation.

Practical Implications

Although the kinetic model described in this publication was derived for a series of experimental austenitic stainless steels, its application can probably be extended to other austenitic alloys by considering the influence of composition on the equilibrium nitrogen content and the desorption rate constant. Further work is needed to determine the influence of welding parameters on nitrogen absorption and desorption.

Acknowledgments

Special thanks to Columbus Stainless for sponsoring the project and performing the nitrogen analyses and the University of Pretoria for providing laboratory facilities. The assistance of Johann Borman and Karin Frost is also gratefully acknowledged.

References

1. Du Toit, M., and Pistorius, P. C. 2003. Nitrogen control during the autogenous arc welding of stainless steel — Part 1: The influence of shielding gas nitrogen content and base metal nitrogen and sulphur concentrations on nitrogen absorption/desorption. *Welding Journal* 82(8): 219-s to 224-s.

2. Katz, J. D., and King, T. B. 1989. The kinetics of nitrogen absorption and desorption from a plasma arc by molten iron. *Metallurgical Transactions B* 20B: 175–185.

3. Bandopadhyay, A., Banerjee, A., and DebRoy, T. 1992. Nitrogen activity determination in plasmas. *Metallurgical Transactions B* 23B: 207–214.

4. Gedeon, S. A., and Eagar, T. W. 1991. Thermochemical analysis of hydrogen absorption in welding. *Welding Journal* 69(7): 264-s to 271-s.

5. Gedeon, S. A. 1987. Hydrogen assisted cracking of high strength steel welds. Ph.D. dissertation, Massachusetts Institute of Technology, Boston, Mass.

6. Kuwana, T., Kokawa, H., and Saotome, M. 1995. Quantitative prediction of nitrogen absorption by steel during gas tungsten arc welding. *Proc. 3rd Int. Seminar Numerical Analysis of Weldability.*

7. Mundra, K., and DebRoy, T. 1995. A general model for partitioning of gases between a metal and its plasma environment. *Metallurgical and Materials Transactions B* 26B: 149–157.

8. Palmer, T. A., and DebRoy, T. 1996. Physical modeling of nitrogen partition between the weld metal and its plasma environment. *Welding Journal* 75(7): 197-s to 207-s.

9. Elliott, J. F., and Gleiser, M. 1963. *Thermochemistry for Steelmaking I.* Reading, Addison-Wesley, p. 75.

10. Kubaschewski, O., Alcock, C. B., and Spencer, P. J. 1993. *Materials Thermochemistry.* Oxford Pergamon Press.

11. Weast, R. C. 1981. *CRC Handbook of Chemistry and Physics.* Boca Raton, Fla.: CRC Press.

12. Reed-Hill, R. E., and Abbaschian, R. 1992. *Physical Metallurgy Principles.* Boston, Mass.: PWS Kent.

13. Wada, H., and Pehlke, R. D. 1977. Solubility of nitrogen in liquid Fe-Cr-Ni alloys containing manganese and molybdenum. *Metallurgical Transactions B* 8B: 675–682.

14. Belton, G. R. 1993. How fast can we go? The status of our knowledge of the rates of gas-liquid metal interactions. *Metallurgical Transactions B* 24B: 241–258.

15. Turkdogan, E. T. 1996. *Fundamentals of Steelmaking.* London, England: The Institute of Materials.

16. The 19th Committee on Steelmaking, The Japan Society for the Promotion of Science. 1988. *Steelmaking Data Sourcebook.* New York, N.Y.: Gordon and Breach.

17. Fruehan, R. J. 1992. Nitrogen control in chromium steels. INFACON 6. *Proc. 1st Int. Chromium Steel and Alloy Congress.* SAIMM, pp. 35–41.

18. Blake, P. D., and Jordan, M. F. 1971. Nitrogen absorption during the arc melting of iron. *Journal of the Iron and Steel Institute*, pp. 197–200.